Portal–Systemic Shunts Reduce Asialoglycoprotein Receptor Density in Rats

Steven D. Colquhoun, Caroline A. Connelly, and David R. Vera

Liver Transplant Program, Department of Surgery, Burns and Allen Research Institute, Cedars-Sinai Medical Center and University of California, Los Angeles; and Department of Radiology, University of California, San Diego, La Jolla, California

The clinical usefulness of quantitative functional imaging techniques that use asialoglycoprotein receptor (ASGP-R) binding is based on the correlation between ASGP-R density and hepatic functional reserve. Portal–systemic shunting (PSS) is common in patients with cirrhosis and portal hypertension—the same group that is most frequently considered for such imaging. PSS occurs spontaneously through collateral vessels and from the creation of surgical shunts or placement of transjugular intrahepatic portal-systemic shunts (TIPS). Understanding the physiologic relationship between PSS and ASGP-R activity may aid in the interpretation of quantitative clinical imaging. This study was conducted to determine the relationship between PSS and ASGP-R density in the absence of parenchymal disease. **Methods:** Sprague-Dawley rats with end-to-side portal-systemic shunts and sham-operated control rats were imaged with ^{99m}Tc-diethylenetriaminepentaacetic acid galactosyl-neoglycoalbumin. Pharmacokinetic modeling of the liver and heart time–activity data was used to measure ASGP-R concentration, as well as hepatic plasma volume and flow. **Results:** The mean ASGP-R density (nmol/g of liver) was significantly decreased in the shunted rats. Blood ammonia was significantly elevated, whereas hepatic plasma flow, alkaline phosphatase, alanine aminotransferase, and aspartate aminotransferase levels were unaltered. Liver histology was normal in both groups. **Conclusion:** A significant change in the ASGP-R density occurs with PSS in the absence of parenchymal disease. PSS appears to be an independent variable affecting ASGP-R activity. This could prove clinically important during interpretation of quantitative imaging from patients with varying degrees of PSS based on underlying disease or the presence of a surgical shunt or TIPS device.

Key Words: ^{99m}Tc-diethylenetriaminepentaacetic acid galactosyl-neoglycoalbumin; hepatic blood flow; liver; quantitative functional imaging

J Nucl Med 2001; 42:110–116

The hepatic binding protein, or hepatocyte-specific human asialoglycoprotein receptor (ASGP-R), is perhaps the best characterized of the receptor-mediated endocytotic systems (*1*). In recent years, ASGP-R expression has been clinically correlated with hepatocyte functional reserve (*2–6*), leading to an increasing interest in imaging techniques using ASGP-R to assess patients with acute or chronic liver disease. In addition to parenchymal disease, several other factors and conditions have been found to influence ASGP-R activity. Portal–systemic shunting (PSS) caused by cirrhosis and portal hypertension is common in patients who may be candidates for this type of imaging. PSS can occur spontaneously through collateral vessels and as a result of surgical or transjugular intrahepatic portal–systemic shunts (TIPS). In many circumstances, the extent of portal hypertension and PSS does not directly correlate with the degree of parenchymal disease. This study sought to explore the possibility of a physiologic relationship between PSS and ASGP-R activity, because any influence can affect the interpretation of quantitative clinical imaging.

Calculating ASGP-R concentration with a radiopharmaceutical mimics methods used clinically and allows accurate assessment of receptor binding in the intact, functioning liver, in contrast to in vitro biochemical approaches that assess receptor binding in homogenized tissue. ^{99m}Tc-labeled galactosyl-neoglycoalbumin and ^{99m}Tc-diethylenetriaminepentaacetic acid galactosyl-neoglycoalbumin (GSA) are both receptor-binding radiopharmaceuticals (*7*) specific for ASGP-R (*8*). A healthy liver will accumulate in excess of 90% of a dose within 15 min, whereas a diseased liver will accumulate significantly less in the same interval (*9*). In this study, a radiopharmacokinetic model (*10*) was used to obtain high-precision measurements (*11*) of ASGP-R concentration (*12,13*) from liver and heart time–activity data (*14*) recorded from rats that underwent portal-systemic shunt or sham (control) operations.

MATERIALS AND METHODS

Animal Preparation

All animals received care in accordance with the National Academy of Sciences guidelines under an institutionally approved protocol. Sprague-Dawley rats (Zivic Laboratories, Pittsburgh, PA) underwent end-to-side portacaval anastomosis under halothane anesthesia (Zivic-Miller Laboratories, Zelionople, PA), with an additional six rats undergoing sham procedures. A midline laparotomy was used to expose the inferior vena cava and portal vein. The inferior vena cava was temporarily occluded above the renal veins, and the portal vein was ligated and divided at the

Received Feb. 22, 2000; revision accepted Jul. 28, 2000.

For correspondence or reprints contact: Steven D. Colquhoun, MD, Cedars-Sinai Medical Center, 8635 W. 3rd St., Ste. 590W, Los Angeles, CA 90048.

hilum. An end-to-side portacaval anastomosis was then performed with medical grade cyanoacrylate adhesive to an appropriate inferior vena cava venotomy. All clips were removed, and the patency of the anastomosis was directly observed. Time-matched sham procedures included laparotomy and transient occlusion of both vessels for the same 5- to 6-min interval required to perform the portacaval shunt. Long-term patency was implied from elevated serum ammonia levels obtained at the time of imaging. The rats were fully recovered and healthy in appearance when studied 72–77 d from the initial surgery. At imaging, the animals were again placed under general anesthesia using chloral hydrate (350 mg/kg intraperitoneally). The femoral veins were cannulated bilaterally for phlebotomy and radiopharmaceutical administration.

Radiopharmacokinetic Model

The detailed methods and assumptions of the radiopharmacokinetic model used for the in vivo measurement of ASGP-R concentration are described in detail elsewhere (*10*). Briefly, ^{99m}Tc-GSA, a radioligand for ASGP-R, was injected into the femoral vein. Images of the heart and liver were then immediately acquired using a standard nuclear medicine computer. Time–activity curves tracing uptake of the ligand into the liver and heart were generated by standard nuclear medicine software and entered into the software program NGAFIT (*6,14*) to calculate receptor concentration. The following parameters were measured using NGAFIT: the ASGP-R concentration $[R]_o$, ASGP-R forward-binding rate constant k_b, hepatic plasma flow F, hepatic plasma volume V_h, and extrahepatic plasma volume V_e. The receptor quantity R_o was calculated from parameters $[R]_o$ and V_h as $R_o = [R]_o V_h$. Scaled values for F, R_o, and V_h were obtained through division by liver weight (lw) and designated $\tilde{F}$, $\tilde{R}_o$, and $\tilde{V}_h$, respectively. The scaled receptor quantity R_o/tbw was calculated as $V_h[R]_o$/tbw. Finally, the maximum receptor transport rate R_{max} was calculated as $k_b[R]_o[R]_o$/tbw (*15*).

Version 6.1 of NGAFIT was designed for measurement of human ASGP-R concentration. The following four modifications to the program were required for measurements from rat time–activity data. First, only the liver time–activity curve was used by NGAFIT. Second, the rat studies used a higher scaled molar dose as well as a smaller injection volume, and the program was altered to reflect these changes. Third, the initial values for plasma volume (V_p) ($= 0.07$ tbw $\times$ pct $\times$ 0.01), V_h ($= 0.237\ V_p$), V_e ($= V_p - V_h$), and F ($= 0.023$ tbw $\times$ pct $\times$ 0.01) were based on total body weight tbw and plasmacrit pct. Fourth, metabolism of the ^{99m}Tc-GSA–ASGP-R complex was included in the model and calculated using an initial rate constant of 0.005/min and a fixed time delay of 12.5 min. This version of NGAFIT was designated 6.1R and executed on a VAX/VMS computer (Digital Equipment Corporation, Maynard, MA).

NGAFIT measures pharmacokinetic parameters by first entering the weight and counts per minute of the 2-min blood sample from the nuclear medicine computer, tbw, and the ^{99m}Tc-GSA galactose density. On the basis of these values, the program sets the initial values for the parameters $[R]_o$, k_b, σ_1, and σ_2 as previously described (*12*) and parameters V_e, V_h, F, and metabolic rate constant. Next, these parameters are adjusted until the model simulation matches the liver time–activity data. On the basis of the quality of this match, the program then determines the technical acceptability of the measurements (*6*). If the quality is found unacceptable, the curve fitting is repeated using the current parameter value as the initial setting for the repeated procedure. Finally, the SD of each measurement is calculated (*16*).

^{99m}Tc-GSA Labeling and Quality Control

GSA was labeled with ^{99m}Tc through tin reduction (*17*). Single-use labeling kits were prepared in the following manner. Freeze-dried Asialoscint (Nihon Medi-Physics, Chiba, Japan) was removed from the multidose vial, and 7.2 mg (containing 0.60 mg or 6.75 nmol GSA) was dispensed into 2-mL vials with a screw cap containing a Teflon (DuPont, Wilmington, DE) septum. The average number of diethylenetriaminepentaacetic acid and galactosyl moieties attached to each albumin molecule was 5 and 32, respectively. After the vials were purged with nitrogen, they were stored at 5°C. The contents of a single vial provided three ^{99m}Tc-GSA doses. Approximately 1110 MBq (~3700 MBq/mL) sodium pertechnetate (DuPont Pharmaceuticals Co., North Billerica, MA) were injected into the vial through the septum. After the solution stood with periodic agitation for 1 h at room temperature, the total volume was brought to 0.60 mL with 0.9% saline. The final ^{99m}Tc-GSA concentration was 1 mg/mL (12.8 nmol/mL). Quality control (*18*) consisted of size-exclusion chromatography (TSK-3000SW [Beckman Instruments, Fullerton, CA], 1 mL/min, 0.9% saline) and required a radiochemical purity in excess of 96%.

^{99m}Tc-GSA Functional Imaging

The hepatic functional imaging study used a standard large-field-of-view gamma camera (ZLC-7500S; Siemens Medical Systems, Hoffman Estates, IL) connected to a nuclear medicine computer (33000; ADAC Laboratories, Milpitas, CA). The gamma camera was fitted with a high-resolution parallel-hole collimator. A symmetric energy window (20%) set at 140 keV was used. A dynamic imaging study (*19*) was acquired at four frames (128 $\times$ 128 $\times$ 8) per minute in $\times$3 zoom mode with the rat supine. ^{99m}Tc-GSA (111–148 MBq, 3.20 nmol/kg) was administered through the femoral vein catheter and was followed by a 1.5-mL saline bolus flush. A timer was started when the radioactivity entered the left ventricle of the heart. A 0.5-mL venous sample was obtained at 2 min after injection from the noninjection catheter. At 20 min after injection, the imaging study was halted and the liver was excised, weighed, and placed in 10% buffered formalin. The 2-min plasma sample and counting standard were assayed for radioactivity (100–200 keV). Time–activity data for the liver were generated using standard nuclear medicine software. The 5-min postinjection image was used to draw a region of interest around the entire liver. The excised livers were sent to an experienced liver pathologist for gross and microscopic examination under masked conditions.

Blood Chemistries

Serum was separated immediately and placed on ice until the following tests were performed, using standard protocols, by the clinical laboratories: ammonia, total bilirubin, glucose, alkaline phosphatase, alanine aminotransferase, and aspartate aminotransferase.

Statistical Analysis

The results are reported as mean $\pm$ SD. An unpaired Student *t* test, using pooled SDs, was used to check for significance between mean values of the shunted and sham-operated groups. Differences were regarded as significant when the two-tailed probability value was 0.05. Statistical analyses were performed with JMP (SAS Institute, Carey, NC) and SPSS (SPSS Inc., Chicago, IL) statistical software.

RESULTS

Figure 1 graphically displays liver function data for both groups. Alkaline phosphatase, alanine aminotransferase, aspartate aminotransferase, and bilirubin levels were not significantly different ($P > 0.05$). The blood ammonia levels of the shunted rats were significantly elevated, confirming shunt patency, whereas blood glucose and the weights of both animals and livers were significantly decreased (Fig. 2).

The functional imaging results indicate decreased ASGP-R binding in the shunted rats compared with the sham-operated rats (Table 1). These measurements included the ASGP-R concentration $[R]_o$, forward-binding rate constant k_b, scaled hepatic plasma flow $\tilde{F}$, receptor density $\tilde{R}_o$, scaled ASGP-R quantity R_o/tbw, maximum receptor transport rate R_{max}, and scaled hepatic plasma volume $\tilde{V}_h$. The mean ASGP-R density $\tilde{R}_o$ in the shunted rats (0.082 ± 0.066 nmol/g of liver) was significantly decreased ($P = 0.012$) compared with the sham-operated rats (0.254 ± 0.119 nmol/g of liver). The scaled hepatic plasma flow of the sham-operated rats was lower than the shunted rats but was not significantly different. A significant difference was observed in scaled hepatic plasma volume. Significantly lower $\tilde{R}_o$ and R_{max} measurements were observed for the shunted rats.

Figure 3 illustrates the typical liver time–activity data with model simulations from a sham-operated rat and a shunted rat. The liver time–activity curve of the shunted rat failed to peak within the 20-min functional imaging study. In contrast, the liver of the sham-operated rat accumulated all of the ^{99m}Tc-GSA within 15 min. The receptor density $\tilde{R}_o$ of the sham-operated rat was 0.286 ± 0.007 nmol/g; the receptor concentration $[R]_o$ was 0.901 ± 0.021 μmol/L. The shunted rat had an $\tilde{R}_o$ of 0.018 ± 0.001 nmol/g and an $[R]_o$ of 0.273 ± 0.001 μmol/L. The receptor density in the two groups is graphically compared in Figure 4.

Figure 5 models how the ^{99m}Tc-GSA liver–activity curves of a sham-operated rat would be altered by diminished hepatic blood flow (A) or decreased receptor concentration (B). Figure 5A depicts simulations with hepatic plasma flow F decreased by 20% (solid line) or 50% (dashed line) while other parameters ($[R]_o$, k_b, V_h, and V_e) remain constant. A 20% change produces an alteration in the time–activity data that is only slightly greater than the data noise, and at 50% the data have yet to approach the diminished uptake of the shunted liver shown in Figure 3. Figure 5B depicts simula-

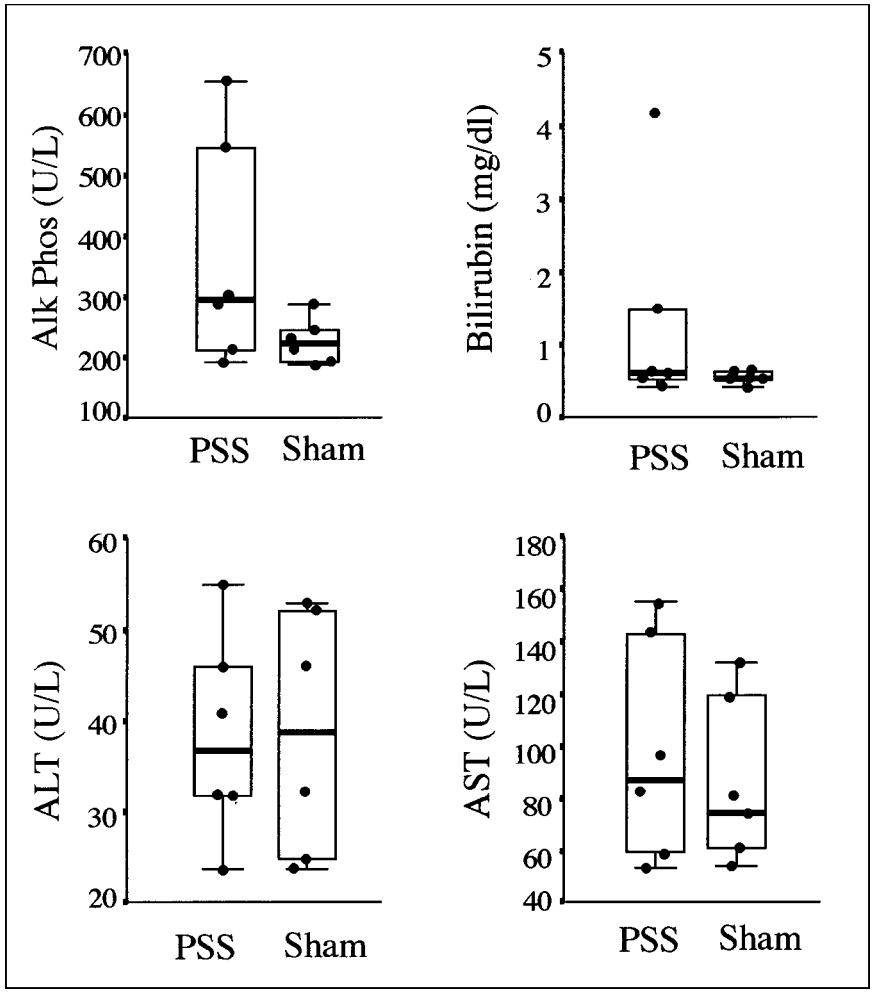

FIGURE 1. Liver enzymes and bilirubin were not significantly different in shunted and sham-operated rats. Top and bottom of each box delineate upper and lower quartile ranges, that is, points containing 25% of data points above and 25% of data points below median. Median is indicated by thicker horizontal line. Error bars are shown above or below each box. Dark circles are data points from individual rats. Alk Phos = alkaline phosphatase; ALT = alanine aminotransferase; AST = aspartate aminotransferase.

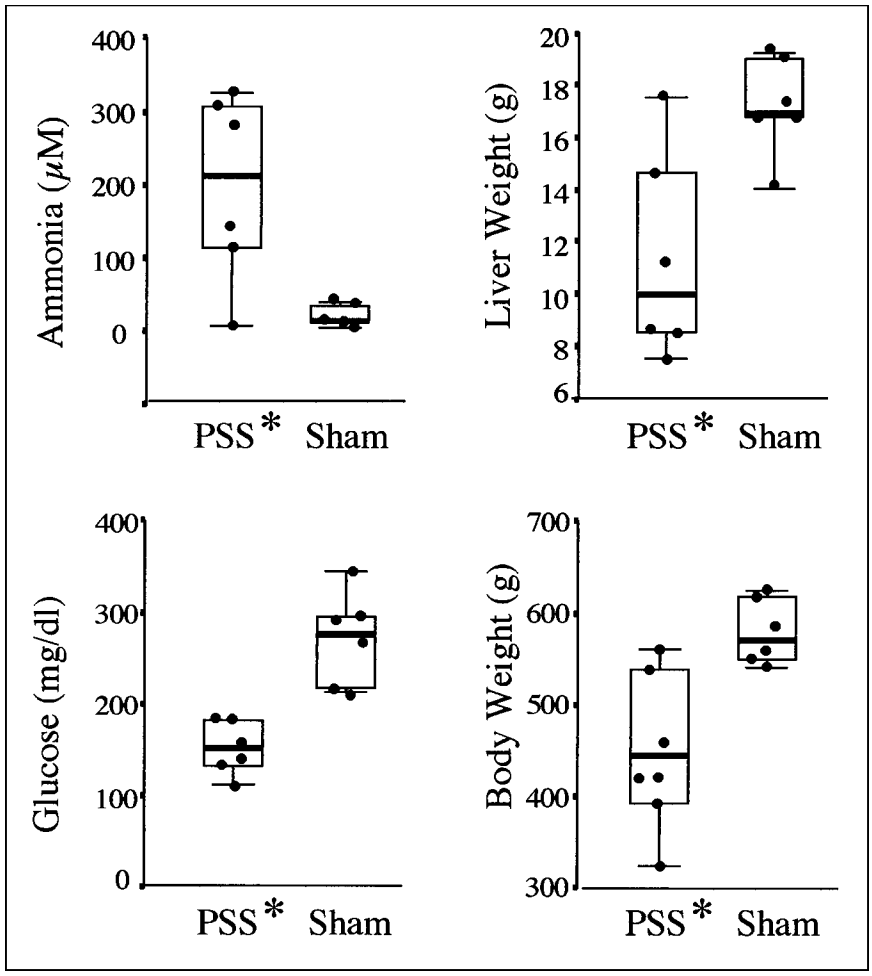

FIGURE 2. Ammonia, glucose, liver, and body weights were significantly different in shunted and sham-operated rats. Top and bottom of each box delineate upper and lower quartile ranges, that is, points containing 25% of data points above and 25% of data points below median. Median is indicated by thicker horizontal line. Error bars are shown above or below each box. Dark circles are data points from individual rats. Asterisks indicate significant differences ($P < 0.05$).

tions produced by a 20% or 50% decrease in receptor concentration with other parameters held constant. The simulated 20% and 50% decreases in receptor concentration more closely correlate with the experimental results seen in Figure 3.

DISCUSSION

Despite the availability of numerous techniques for assessing hepatic reserve, few are both accurate and clinically useful. Standard tests such as indocyanine green metabolism, the arterial-to-ketone body ratio (*20*), lidocaine–monoethylglycinexylidide testing, the Childs-Pugh score, aminopyrine breath testing, and biochemical estimates of synthetic function are all either inadequate or too cumbersome for routine clinical use. Yet such information can be of significant interest when, for example, contemplating a surgical resection in a patient with chronic disease or cirrhosis. Without adequate functional reserve, which we define as the

TABLE 1
Functional Imaging Results

Parameter	Symbol	PSS	Sham	*P*
Receptor concentration (μmol/L)	$[R]_o$	0.366 ± 0.138	0.683 ± 0.323	0.052
Forward binding rate constant (L/μmol per minute)	k_b	0.972 ± 0.730	1.859 ± 0.901	0.090
Hepatic plasma flow/liver weight (mL/min/g)	$\tilde{F}$	0.676 ± 0.437	0.355 ± 0.123	0.114
Receptor/liver weight (nmol/g)	$\tilde{R}_o$	0.082 ± 0.066	0.254 ± 0.119	0.012
Receptor/rat weight (pmol/g)	R_o/tbw	2.11 ± 1.85	7.53 ± 3.57	0.008
Maximum transport rate (nmol/L per min/g)	R_{max}	0.384 ± 0.501	1.686 ± 1.113	0.027
Hepatic plasma volume/liver weight (mL/g)	$\tilde{V}_h$	0.213 ± 0.144	0.388 ± 0.087	0.029

ASGP-R density ($\tilde{R}_o$) significantly decreased in PSS rats, with no change in hepatic plasma flow/liver weight ($\tilde{F}$). Statistical comparisons of other parameters measured in PSS ($n = 6$) and sham-operated ($n = 6$) rats are also indicated.

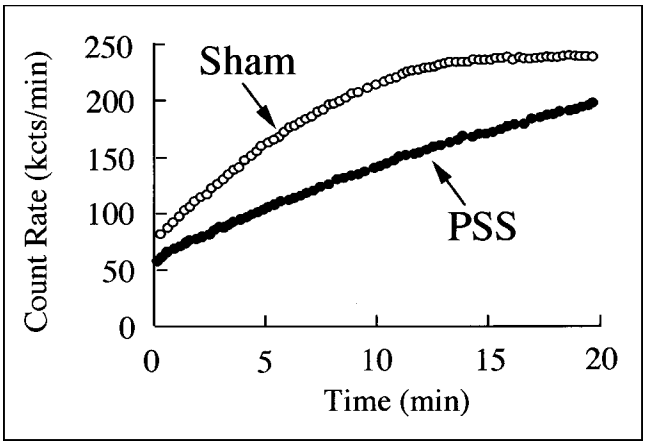

FIGURE 3. Liver time–activity data with model simulations from two representative studies: sham-operated rat and shunted rat. $\tilde{R}_o$ of sham-operated rat was 0.286 ± 0.007 nmol/g; receptor concentration $[R]_o$ was 0.901 ± 0.021 μmol/L. Shunted rat had $\tilde{R}_o$ of 0.018 ± 0.001 nmol/g and $[R]_o$ of 0.273 ± 0.001 mol/L. kcts = kilocounts.

current metabolic capacity, an otherwise successful resection can lead to liver failure.

Radiopharmaceuticals are known for their marked sensitivity, allowing detection of biochemical abnormalities before anatomic changes. In recent years, interest has been increasing about imaging techniques using ASGP-R, which appears to correlate with hepatic reserve (*2–6*). Early on,

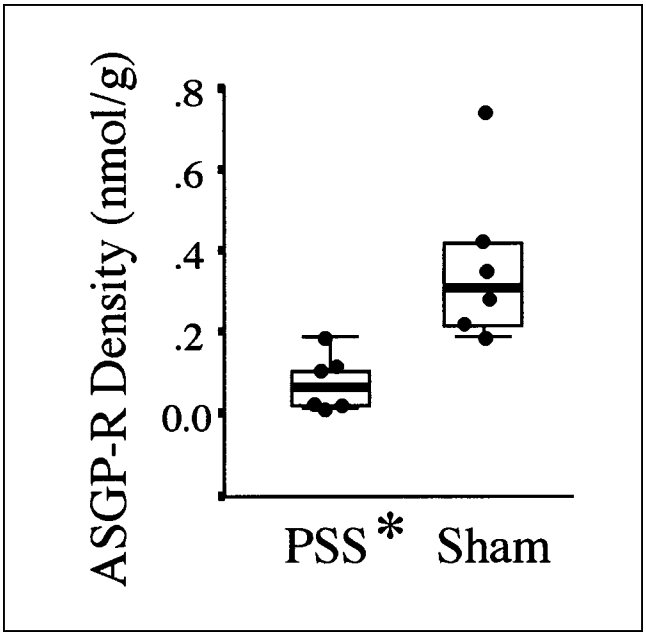

FIGURE 4. Representation of ASGP-R $\tilde{R}_o$ for shunted and sham-operated rats. Top and bottom of each box delineate upper and lower quartile ranges, that is, points containing 25% of data points above and 25% of data points below median. Median is indicated by thicker horizontal line. Error bars are shown above or below each box. Dark circles are data points from individual rats. Asterisk indicates significant differences ($P < 0.05$).

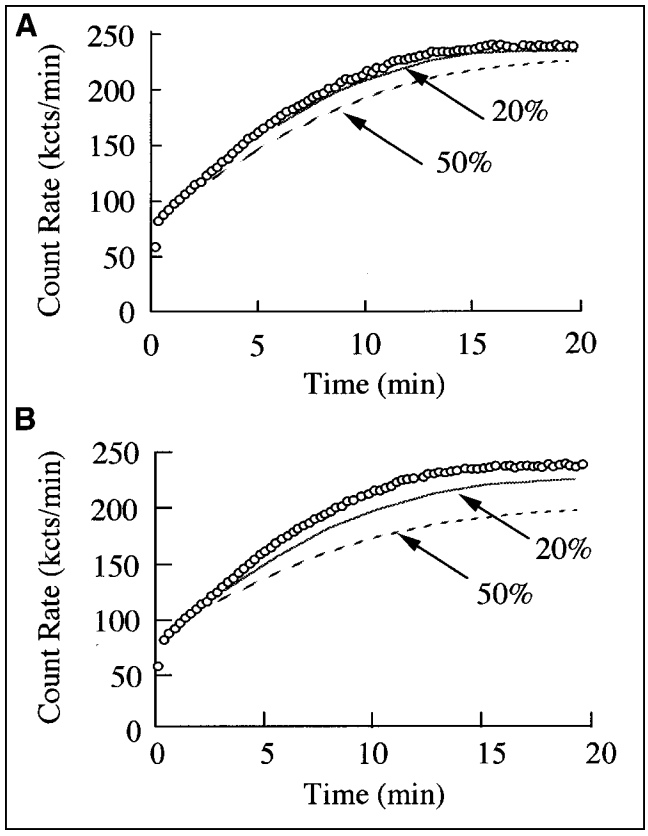

FIGURE 5. (A) Simulated changes in ^{99m}Tc-GSA liver–activity curve if hepatic blood flow is reduced by 20% (solid line) or 50% (dashed line). (B) Simulated changes in ^{99m}Tc-GSA liver–activity curve if receptor concentration is reduced by 20% (solid line) or 50% (dashed line). ^{99m}Tc-GSA liver time–activity data from sham-operated rat are indicated by circles. kcts = kilocounts.

Sawamura et al. (*21*) examined liver biopsy specimens obtained from patients with cirrhosis or hepatocellular carcinoma, comparing these specimens with specimens from patients with no liver disease. In patients with cirrhosis, the ASGP-R activity was found to be only 28% of that seen in healthy volunteers, and activity was negligible in patients with a tumor. In a more recent study, functional imaging was used to assess 51 patients with chronic liver disease and 18 with acute abnormalities (*22*). An excellent correlation was found between functional imaging and multiple conventional testing criteria. Other studies have since shown favorable comparisons between ASGP-R imaging and both indocyanine green and aminopyrine breath tests (*4,6*). Yumoto et al. (*23*) have carried this further by using functional imaging to estimate the proposed remnant liver function before hepatectomy. Through follow-up of patients after resection, an apparent threshold of activity was determined below which severe postoperative dysfunction occurred. Kwon et al. (*24*) have reported the use of ^{99m}Tc-GSA scintigraphy in 90 patients undergoing elective hepatectomy. In that report, the results of conventional liver function studies, indocyanine green retention, and ^{99m}Tc-GSA scintigraphy were compared with histologic findings from

resected specimens. Scintigraphy correlated best with both histologic findings and clinical outcomes. Interestingly, in those instances in which indocyanine green and ^{99m}Tc-GSA did not correlate well, the possible cause of the differences was thought to have been intrahepatic and extrahepatic shunting.

The results of this study suggest that PSS can significantly influence ASGP-R activity. In principle, ASGP-R activity can be influenced at many levels, including receptor transcription, translation, cotranslation, posttranslation, expression, membrane distribution, zonal distribution, binding, and endocytosis, as well as intracellular trafficking and recycling (*1*,*25*,*26*). As alluded to earlier, a host of agents and other conditions have already been correlated with changes in ASGP-R expression. For example, ethanol has been found to impair ligand binding in the process of receptor-mediated endocytosis (*27*). This impairment appears specific for hepatocytes and controls the selective uptake and degradation of serum asialoglycoproteins with terminal galactose or *N*-acetyl-galactosamine residues. The impairment begins acutely as an inactivation of the receptor, followed later by redistribution and, finally, decreased production (*28*,*29*). Such a disruption of receptor-mediated endocytosis is a potential mechanism underlying the reduced ASGP-R expression observed in the PSS model. In fact, autopsy series of cirrhotic patients have documented alterations in ASGP-R distribution (*30*). Other conditions, such as protein malnutrition, have also been correlated with as much as a 66% reduction in ASGP-R (*31*). Certain drugs, such as the antimalarial drug chloroquine, may also reduce receptor activity (*32*). Some drugs, such as vasopressin or ursodeoxycholate, commonly administered to patients with liver disease could also affect ASGP-R activity (*33*,*34*).

The underlying mechanism for the observed difference in ASGP-R activity in sham-operated and shunted animals is not clear. One plausible explanation could be based on a simple decrease in hepatic blood flow. Although a diminished hepatic plasma flow can contribute to a slower extraction of ^{99m}Tc-GSA, we know through simulations that an isolated change in flow cannot account for a decreased uptake of such magnitude (Fig. 5). The curves in Figure 5 clearly show the relative sensitivity of liver uptake to changes in hepatic plasma flow and receptor concentration. When uptake requires more than 15 min for complete extraction, the target tissue is insensitive to changes in plasma flow but extremely sensitive to the factors influencing receptor binding. Alternatively, it could be argued that shunted animals manifest severe parenchymal injury inflicted by the shunt itself. Several studies have already documented the physiologic changes that occur after the creation of a portacaval shunt. These include a decreased body weight and hyperammonia, both of which were seen in this study (*35*). Some postshunt hepatic atrophy also occurs, but with preservation of hepatic regenerative potential (*36*). Interestingly, no gross or histologic changes occur as a result of portacaval shunting alone (*35*–*37*). Indeed, no histologic differences were noted between the two groups in this study. With the exception of a slightly lower body weight, shunted animals were grossly both physically and behaviorally indistinguishable from sham-operated animals. No detectable differences in biochemical findings were observed, aside from the expected alterations in ammonia and glucose consistent with shunt patency. A portacaval shunt per se is well tolerated by an otherwise normal liver. As a further illustration, patients with isolated portal vein thrombosis caused by trauma or childhood disease are known to have normal liver histology and function (*38*).

With the general acceptance of the TIPS procedure, the number of patients with such devices has risen dramatically while surgical creation of shunts has fallen sharply. Interestingly, the long-term physiologic changes to the liver are likely to be similar. Crippin et al. (*39*) have shown that in appropriately selected candidates, little change occurs in hepatic biochemical profiles with TIPS placement.

Although portal hypertension and intrinsic shunting occur in the context of cirrhosis, the degree of PSS does not always correlate with the severity of parenchymal disease (*40*). Patients with end-stage liver disease from any cause can present with widely varying degrees of PSS. If PSS is an independent variable affecting ASGP-R activity, then clinically, the degree of PSS may be important to consider when one is interpreting the results of functional imaging. In fact, to our knowledge this is the first study to isolate PSS from parenchymal disease in the use of ASGP-R functional imaging.

CONCLUSION

Our results confirm that ASGP-R binding kinetics are significantly altered after portacaval shunting in rats, despite the absence of significant intrinsic parenchymal disease. These changes in binding kinetics are not caused simply by changes in blood flow brought about by the shunt. PSS, therefore, appears to represent an independent variable influencing ASGP-R activity, suggesting that ASGP-R imaging in the presence of PSS may lead to underestimation of true hepatic reserve. The magnitude of PSS, including spontaneous collaterals, surgical shunts, and TIPS, should be considered during interpretation of ASGP-R functional imaging results. Future studies assessing the relationship between ASGP-R functional imaging and shunt fraction are needed. Such considerations may further improve the correlation between ASGP-R functional imaging and clinical outcome.

ACKNOWLEDGMENTS

The authors thank Dr. Boris Rubner and Dr. Lidija Petrovic for assistance with histologic comparisons, Dusan P. Hutak for technical assistance, and Nihon Mediphysics for the gracious donation of the ^{99m}Tc-GSA kits. This study was supported in part by U.S. Public Health Service grant

AM34758 and a grant from the American Lung Association of California, Oakland, CA.

REFERENCES

1. Ashwell G, Steer CJ. Hepatic recognition and catabolism of serum glycoproteins. *JAMA*. 1981;246:2358–2364.
2. Virgolini I, Müller C, Klepetko W, et al. Decreased hepatic function in patients with hepatoma or liver metastasis monitored by a hepatocyte-specific galactosylated radioligand. *Br J Cancer*. 1990;61:937–941.
3. Virgolini I, Müller C, Höbart J, et al. Liver function in acute viral hepatitis as determined by a hepatocyte-specific ligand: ^{99m}Tc-galactosyl-neoglycoalbumin. *Hepatology*. 1992;15:593–598.
4. Kudo M, Todo A, Ikekubo K, Yamamoto K, Vera DR, Stadalnik RC. Quantitative assessment of hepatocellular function via in vivo radioreceptor imaging: technetium-99m-galactosyl human serum albumin (Tc-GSA). *Hepatology*. 1993; 17:814–819.
5. Virgolini I, Kornek G, Höbart J, et al. Scintigraphic evaluation of functional hepatic mass in patients with advanced breast cancer. *Br J Cancer*. 1993;68:549–554.
6. Pimstone NR, Stadalnik RC, Vera DR, Hutak DP, Trudeau WL. Evaluation of hepatocellular function via receptor-mediated uptake of a technetium-99m-labeled asialoglycoprotein analogue. *Hepatology*. 1994;20:917–923.
7. Stadalnik RC, Kudo M, Eckelman WC, Vera DR. In vivo functional imaging using receptor-binding radiopharmaceuticals: technetium-99m-galactosyl-neoglycoalbumin as a model. *Invest Radiol*. 1993;28:64–70.
8. Stockert RJ, Morell AG. Hepatic binding protein: the galactose-specific receptor of mammalian hepatocytes. *Hepatology*. 1983;3:750–757.
9. Stadalnik RC, Vera DR, Woodle ES, et al. Technetium-99m NGA functional hepatic imaging: preliminary clinical experience. *J Nucl Med*. 1985;26:1233–1242.
10. Vera DR, Krohn KA, Stadalnik RC, Scheibe PO. Tc-99m galactosyl-neoglycoalbumin: in vivo characterization of receptor-mediated binding. *J Nucl Med*. 1984;25:779–787.
11. Vera DR, Krohn KA, Scheibe PO, Stadalnik RC. Identifiability analysis of an in vivo receptor-binding radiopharmacokinetic system. *IEEE Trans Biomed Eng*. 1985;BME-32:312–322.
12. Kudo M, Vera DR, Trudeau WL, Stadalnik RC. Validation of in vivo receptor measurements via in vitro radioassay: technetium-99m-galactosyl-neoglycoalbumin as a prototype model. *J Nucl Med*. 1991;32:1177–1182.
13. Kudo M, Vera DR, Trudeau WL, Stadalnik RC. Hepatic uptake of [^{99m}Tc]galactosyl-neoglycoalbumin is sensitive to receptor quantity. *Nucl Med Biol*. 1991;18: 663–666.
14. Vera DR, Stadalnik RC, Trudeau WL, Scheibe PO. Measurement of receptor concentration and forward binding rate constant via radiopharmacokinetic modeling of [^{99m}Tc]galactosyl-neoglycoalbumin. *J Nucl Med*. 1991;32:1169–1176.
15. Vera DR, Stadalnik RC, Metz CE, Pimstone NR. Diagnostic performance of a receptor-binding radiopharmacokinetic model. *J Nucl Med*. 1996;37:160–164.
16. Vera DR, Scheibe PO, Banin Y, Stadalnik RC. Local identifiability of a receptor-binding radiopharmacokinetic system having measured parameters of known uncertainty. *IEEE Trans Biomed Eng*. 1994;41:891–897.
17. Kudo M, Washino K, Yamamichi Y, Ikekubo K. Synthesis and radiolabeling of galactosyl human serum albumin. In: Lee YC, Lee RT, eds. *Methods in Enzymology*. Vol 247. San Diego, CA: Academic Press; 1994:383–394.
18. Vera DR, Stadalnik RC, Krohn KA. [Tc-99m]galactosyl-neoglycoalbumin: preparation and preclinical studies. *J Nucl Med*. 1985;26:1157–1167.
19. Vera DR, Krohn KA, Stadalnik RC, Scheibe PO. [Tc-99m]galactosyl-neoglycoalbumin: in vivo characterization of receptor-mediated binding to hepatocytes. *Radiology*. 1984;151:191–196.
20. Matsushita K, Kawasaki S, Makuuchi M. Arterial ketone body ratio in liver surgery. *Hepatology*. 1994;20:331–335.
21. Sawamura T, Nakada H, Hazama H, Shiozaki Y, Sameshima Y, Tashiro Y. Hyperasialoglycoproteinemia in patients with chronic liver diseases and/or liver cell carcinoma: asialoglycoprotein receptor in cirrhosis and liver cell carcinoma. *Gastroenterology*. 1984;87:1217–1221.
22. Kudo M, Todo A, Ikekubo K, Hino M. Receptor index via hepatic asialoglycoprotein receptor imaging: correlation with chronic hepatocellular damage. *Am J Gastroenterol*. 1992;87:865–870.
23. Yumoto Y, Umeda M, Ohshima K, et al. Estimation of remnant liver function before hepatectomy by means of technetium-99m-diethylenetriamine-pentaacetic acid galactosyl human albumin. *Cancer Chemother Pharmacol*. 1994;33(suppl):S1–S6.
24. Kwon AH, Ha-Kawa SK, Uetsuji S, Inoue T, Matsui Y, Kamiyama Y. Preoperative determination of the surgical procedure for hepatectomy using technetium-99m-galactosyl human serum albumin (^{99m}Tc-GSA) liver scintigraphy. *Hepatology*. 1997;25:426–429.
25. Stockert RJ. Regulation of the human asialoglycoprotein receptor by cAMP. *J Biol Chem*. 1993;268:19540–19544.
26. Voorschuur AH, Kuiper J, Neelissen JA, Boers W, VanBerkel TJ. Different zonal distribution of the asialoglycoprotein receptor, the a2-macroglobulin receptor/low-density-lipoprotein receptor-related protein and the lipoprotein-remnant receptor of rat liver parenchymal cells. *Biochem J*. 1994;303:809–816.
27. Clemens DL, Halgard CM, Cole JR, Miles RM, Sorrell MF, Tuma DJ. Impairment of the asialoglycoprotein receptor by ethanol oxidation. *Biochem Pharmacol*. 1996;52:1499–1505.
28. Tworek BL, Tuma DJ, Casey CA. Decreased binding of asialoglycoproteins to hepatocytes from ethanol-fed rats. *J Biol Chem*. 1996;271:2531–2538.
29. Kohgo Y, Mogi Y, Kato J, et al. Ethanol inhibits asialoglycoprotein receptor synthesis but augments its mRNA expression in human hepatoma cell line. *J Gastroenterol*. 1994;29:598–604.
30. Burgess JB, Baenziger JU, Brown WR. Abnormal surface distribution of the human asialoglycoprotein receptor in cirrhosis. *Hepatology*. 1992;15:702–706.
31. Reif S, El-Bendary M, Bujanover Y, Petell JK, Lebenthal E. Protein-restricted diet alters concentration of plasma membrane glycoproteins in rat liver. *J Gastroenterol*. 1996;31:546–551.
32. Tolleshaug H, Berg T. Chloroquine reduces the number of asialo-glycoprotein receptors in the hepatocyte plasma membrane. *Biochem Pharmacol*. 1979;28: 2919–2922.
33. Gil-Falgon S, Lamaze C, Hacein-Bey S, Feger J. Effects of vasopressin on receptor-mediated endocytosis of asialoglycoprotein by hepatocytes from normal and diabetic rats. *Exp Cell Res*. 1992;199:223–228.
34. Kren BT, Rodrigues CM, Setchell KD, Steer CJ. Posttranscriptional regulation of mRNA levels in rat liver associated with deoxycholic acid feeding. *Am J Physiol*. 1995;269:G961–G973.
35. Herz R, Sautter V, Robert F, Bircher J. The Eck fistula rat: definition of an experimental model. *Eur J Clin Invest*.1972;2:390–397.
36. Fisher B, Fisher ER, Lee S. Experimental evaluation of liver atrophy and portacaval shunt. *Surg Gynecol Obstet*. 1967;125:1253–1258.
37. Robson SC, Jaskiewicz K, Engelbrecht G, Kahn D, Hickman R, Kirsch RE. Haemostatic and immunologic sequelae of portacaval shunt in rats. *Liver*. 1995; 15:293–299.
38. Orloff MJ, Orloff MS, Rambotti M. Treatment of bleeding esophagogastric varices due to extrahepatic portal hypertension: results of portal-systemic shunts during 35 years. *J Pediatr Surg*. 1994;29:142–151
39. Crippin JS, Schmidt RD, Niblett RL, Rees CR. Effect of a transjugular intrahepatic portosystemic shunt on liver biochemical profiles. *J Vasc Intervent Radiol*. 1995;6:461–464.
40. Kasai T, Moriwaki H, Okuno M, et al. The clearance rate of chylomicron retinyl ester from plasma can be used to distinguish rats with cirrhosis from those with portacaval shunt. *Hepatology*. 1993;17:125–130.